Understanding Electronic Effects on Carboxylate-Assisted C–H Activation at Ruthenium: The Importance of Kinetic and Thermodynamic Control.

Raed A Alharis,[§,a] Claire L. McMullin,[†,b] David L. Davies,*[,a] Kuldip Singh,[a] and Stuart A. Macgregor.*[,b]

[a]Department of Chemistry, University of Leicester, Leicester, LE1 7RH, UK.

[b]Institute of Chemical Sciences, Heriot-Watt University, Edinburgh, EH14 4AS, UK.

[§]Department of Chemistry, College of Education for Pure Sciences, University of Basrah, Basrah, Iraq.

[†]Present address: Department of Chemistry, University of Bath, Bath, BA2 7AY, UK.

Abstract

Meta- and *para*-substituted 1-phenylpyrazoles (R-phpyz-H) react with $[RuCl_2(p\text{-cymene})]_2$ in the presence of NaOAc to form cyclometallated complexes [M(R-phpyz)Cl(*p*-cymene)] (where R = NMe_2, OMe, Me, H, F, CF_3 and NO_2). Experimental and DFT studies indicate that product formation can be reversible or irreversible depending on the substituents and the reaction conditions. Competition experiments show that the kinetic selectivity favors electron-donating substituents and correlate well with the Hammett parameter giving a negative slope (ρ = -2.4) that is consistent with a cationic transition state. However, surprisingly, the thermodynamic selectivity is completely opposite, with substrates with electron-withdrawing groups being favored. These trends are reproduced with DFT calculations that locate rate-limiting transition state dominated by Ru–O bond dissociation and minimal C–H bond elongation. Detailed computational analysis of these transition states shows that C–H activation proceeds by an AMLA/CMD mechanism through a synergic combination of a C–H→Ru agostic interaction and C–H···O H-bonding. NBO calculations also highlight a syndetic bonding term, and the relative weights of these three components vary in a complementary fashion depending on the nature of the substituent. With *meta*-substituted ligands H/D exchange experiments signal kinetically accessible *ortho*-C–H activation when R = NMe_2, OMe and Me. This is also modelled computationally and the calculations also highlight the kinetic relevance of the HOAc/Cl exchange that occurs post C–H bond cleavage, in particular with the bulkier NMe_2 and Me substituents. Our study highlights that the experimental substituent effects are dependent on the reaction conditions and so using such studies to assign the mechanism of C–H activation in either stoichiometric or catalytic reactions may be misleading.

Introduction.

The use of Ru catalysts in combination with carboxylate salts has become a popular basis for the catalytic functionalisation of aromatic C–H bonds.[1,2,3,4] Such systems generally involve an initial C–H activation step, usually[5] mediated by a directing group to form an *ortho*-cyclometallated intermediate that can react on with a coupling partner to produce a variety of heterocyclic or C–H functionalised products. The mechanisms of the C–H activation processes within these catalytic systems are routinely probed using both experimental and computational methods, often most powerfully when both approaches are used in combination.[6] Experimentally, the reversibility of the C–H activation step is addressed via H/D exchange reactions (both with and without the coupling partner being present) and k_H/k_D kinetic isotope effect (KIE) experiments can shed light on the kinetic relevance of the C–H activation process within the overall catalytic cycle.

Computational methods perhaps provide the most direct way to interrogate the intimate nature of the carboxylate-assisted C–H bond activation process. Over the years a large number of studies[7] have characterised a base-assisted C–H cleavage at a variety of metals, whereby interaction of the C–H bond with an electron deficient metal centre renders the C–H bond susceptible to cleavage by a chelating carboxylate base.[3-4, 8] Fagnou called this process 'Concerted Metallation Deprotonation' (CMD)[9] and we also introduced the term 'Ambiphilic Metal-Ligand Assistance' (AMLA)[7a] to emphasize the dual role of metal centre and chelating base in effecting C–H bond cleavage. We have argued that when the base is bound to the metal centre AMLA and CMD are essentially the same process and in the following we will use these two terms in conjunction (see Figure 1). Previously, Ess and Goddard had coined the term 'Internal Electrophilic Substitution' to describe related processes at $Ir(acac)_2(OR)$ fragments (R = Me, C(O)Me; acac = acetylacetonate).[10] This places more emphasis on the contribution of the electrophilic metal centre and has subsequently been extended to 'Base-assisted Internal Electrophilic Substitution' (BIES), which acknowledges the important role played by the base.

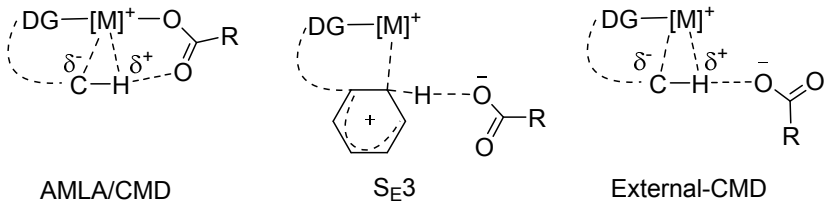

Figure 1. Proposed transition states for C–H activation using internal and external carboxylate-assisted bases.

Two experimental kinetic studies on carboxylate-assisted C–H activation at Ru have been reported by Dixneuf and Jutand and co-workers. Using pre-formed [Ru(OAc)$_2$(*p*-cymene)] they proposed that the cyclometallations of 2-phenylpyridine,[11] 2-phenylpyrazole and 2-phenyl-2-oxazoline[12] in acetonitrile involved an autocatalytic process, whereby the acetic acid released in the reaction facilitates acetate dissociation in the bis-acetate precursor. On the basis of a rate-enhancement observed upon adding acetate, the C–H bond cleavage event was proposed to involve an S_E3 process involving an external acetate base (Figure 1). Similar external deprotonation processes have also been found to be favoured computationally at Ru,[4a,13] although in general computational studies have tended to focus on the intramolecular pathway. An alternative interpretation of the S_E3 reaction is that the external base acts to deprotonate an agostic C–H bond, and we have termed such reactions external-CMD.[7b] These two views of external deprotonation have parallels in the discussion of internal deprotonation processes as proceeding via agostic (AMLA/CMD) or Wheland (S_EAr) intermediates.[14]

Against this complex mechanistic backdrop, aromatic substrate substituent effects have been widely used as an experimental means to elucidate the nature of the carboxylate-assisted C–H cleavage step. For Ru many catalytic systems have been assessed in this way, often by a competition reaction between two substrates, one with an electron-withdrawing substituent and one with an electron-releasing substituent. Several examples have been reported where electron-releasing substituents enhance the reaction efficiency,[4b, 15] and such observations have been taken as evidence for a BIES mechanism over AMLA/CMD.[15f] In other, apparently related systems, electron withdrawing substituents have been shown to enhance reactivity,[16,17] while in some cases no significant substituent effect is seen.[18,15e] This apparent dichotomy in selectivity is not new and nor is it restricted to Ru. As long ago as 2008, Fagnou and Gorelsky showed that the rates of direct arylation reactions at Pd could be enhanced (relative to benzene) for substrates fitted with *either* electron-rich *or* electron-withdrawing substituents.[19] They were subsequently able to rationalise these observations in terms of an activation strain model that showed electron-poor substrates exhibited less distortion in the transition state, whereas electron-rich substrates benefitted from better interaction with the metal centre.[20] We subsequently demonstrated different selectivities in the reactions of 1-(aryl)-methanimine substrates at $[MCl_2Cp^*]_2$ dimers depending on whether the reaction was under thermodynamic (M = Rh) or kinetic (M = Ir) control.[21] Very recently we have also shown how the same C–H activation reaction at a given metal centre can exhibit opposing substituent effects depending on the reaction conditions.[22] Thus the acetate-assisted cyclometallations of *para*- and *meta*-substituted 1-phenylpyrazoles at $[MCl_2Cp^*]_2$ dimers (M = Rh, Ir) each exhibit a negative Hammett plot that reflects rate enhancement with electron-releasing substituents. However, the same reactions can favour products with electron withdrawing substituents upon heating to achieve equilibrium. A single reaction can therefore show opposing substituent effects depending on whether the process is under kinetic or thermodynamic control. This has important implications for the

interpretation of the mechanisms of C–H activation, both as a stoichiometric process and within a catalytic cycle.

In this paper we extend our previous study on the reactivity of $[MCl_2Cp^*]_2$ dimers (M = Rh, Ir) to the isoelectronic $[RuCl_2(p\text{-cymene})]_2$ system. Through a combination of experimental and DFT studies we demonstrate apparently contradictory substituent effects in the cyclometallation reactions of 1-phenylpyrazoles. The interpretation of these observations is readily understood in terms of kinetic and thermodynamic control of reactivity and DFT calculations are employed to support these conclusions and provide insight into the details of the C–H activation step that proceeds by an AMLA/CMD process.

Results and Discussion

Reactions of the *para*-substituted 1-phenylpyrazole ligands (**L1-R**) with $[RuCl_2(p\text{-cymene})]_2$, in MeOH or a mixture of DCM and MeOH in the presence of NaOAc gave the meta-substituted compounds **1-R** (Scheme 1A). The corresponding meta-substituted ligands **L2-R** have two possible sites for cyclometallation giving rise to *ortho*- or *para*-substituted products (**2-R** and **3-R** respectively Scheme 1B). All the compounds were fully characterized by ^{1}H and ^{13}C NMR spectroscopy and in several cases by X-ray crystallography (See ESI). Complex **1-H** has been reported previously.[23]

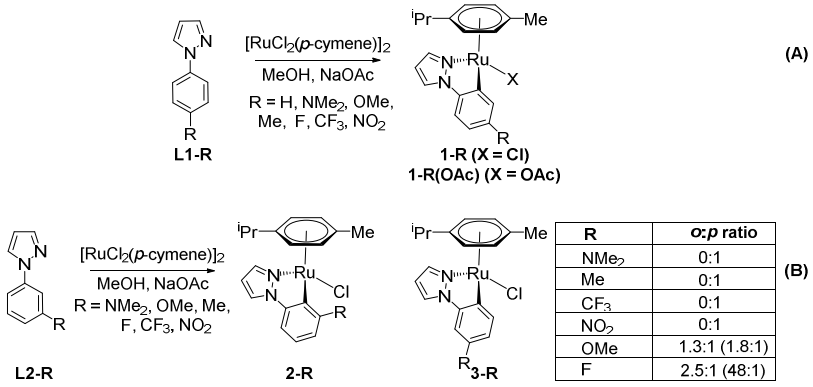

R	*o*:*p* ratio
NMe_2	0:1
Me	0:1
CF_3	0:1
NO_2	0:1
OMe	1.3:1 (1.8:1)
F	2.5:1 (48:1)

Scheme 1. Preparation of (A) *meta*-substituted cyclometallated complexes **1-R**, (B) *ortho*- and/or *para*-cyclometallated complexes **2-R** and **3-R**. Reactions were carried out at room temperature as standard. Ratios in parentheses were obtained after heating at 50 °C in MeOH/DCM (1:4).

The ^{1}H NMR spectra of **1-R** show that the A_2B_2 system from the *para*-substituted phenyl in the free ligand disappears due to cyclometallation. In addition the four aromatic protons of the *p*-cymene become inequivalent as do the two methyl groups of the isopropyl consistent with the Ru atom becoming chiral.

Monitoring the reactions by ^{1}H NMR spectroscopy often showed the presence of [RuCl(OAc)(*p*-cymene)][24] (<20%) after relatively short periods of time. This gradually reduced as the reaction

progressed though sometimes even at long reaction times some remained. In addition, unlike reactions with $[MCl_2Cp^*]_2$ (M = Ir, Rh) which gave just one cyclometallated product, reactions with $[RuCl_2(p\text{-cymene})]_2$ often gave a second product believed to be an acetate coordinated species **1-R(OAc)** which disappeared over time. This was confirmed with **L1-H** by using two equivalents of acetate per Ru that gave rise to two products in a 1:1 ratio after 15 minutes. After 24 hours the ratio had changed to 1:6.9 favouring the chloride product **1-H**. Addition of LiCl to the NMR sample converted the remaining **1-H(OAc)** to **1-H**. Hence when monitoring reactions LiCl was routinely added to the NMR sample to reduce the number of species present.

As found for $[MCl_2Cp^*]_2$ (M = Ir, Rh)[22] reactions with electron-donating substituents were faster. The reaction with **L1-NMe$_2$** reached 85% conversion in 3 hours, **L1-F** reached 93% conversion in 21 hours whilst **L1-NO$_2$** required heating at 40 °C for 96 hours to give a conversion of 75%. The reactions with *meta*-substituted ligands **L2-R** gave only the *para* isomer **3-R** except when R = OMe or F for which a mixture of isomers was formed with the *ortho* isomer **2-R** being slightly favoured. As found previously for the corresponding Cp*Rh complexes, the *ortho*:*para* ratio changed over time. This suggests that these reactions are reversible (see deuteration below). For both **L2-R** (R = OMe, F) the *ortho* isomer becomes more favoured over time; for R = F heating at 50 °C led to a 48:1 ratio in favour of the *ortho* isomer. Fairlamb et al. showed that cyclometallation of fluorinated dimethylbenzylamines with $PdCl_2$ gave exclusively the *para*-isomer, whereas use of $Pd(OAc)_2$ led to formation of a mixture of *ortho*- and *para*-isomers. They attributed this difference to a change in mechanism of C–H activation from S_EAr with $PdCl_2$ to AMLA/CMD with $Pd(OAc)_2$. Fairlamb et al. recently suggested that formation of the *ortho* isomer in the cyclometallations of fluorinated dimethylbenzylamines at Pd was evidence for a CMD/AMLA mechanism.[25]

Several of the cyclometallated products (**1-R**, R = OMe, F, CF_3 and NO_2; **2-F**) were suitable for X-ray diffraction and the structures all show the expected piano stool geometry with the *p*-cymene ring bonded asymmetrically to the metal center with two long Ru—C bonds [2.24 – 2.29 Å] (*trans* to the cyclometallated bond, Ru—C(9)) and four short ones [2.15 – 2.23 Å] (see Figure S1 for structures and Table S1 for selected bond lengths and angles). For the *meta*-substituted complexes, **1-R**, the Ru—C(9) bond length is statistically the same in all the complexes [2.055(6) - 2.069(3) Å] whilst in *ortho* complex **2-F** it is slightly longer [2.082(3) Å].

As mentioned above changes in *ortho*:*para* ratios suggest that at least some of the reactions are reversible. This was probed by deuteration experiments, see Scheme 2. For ligands **L1-R** sites A and B are equivalent whereas for **L2-R** site A corresponds to formation of the *ortho* isomer and site B formation of the *para* isomer.

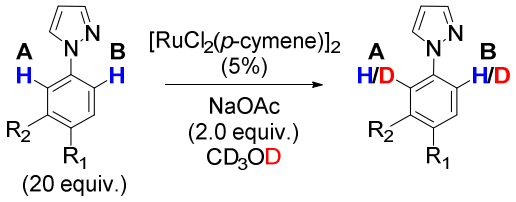

			A	B	time
1	R_1	NMe_2	15%	15%	16 days
2	R_1	OMe	ND	ND	10 days
3	R_2	NMe_2	8%	50%	2 hours
4	R_2	OMe	15%	15%	4 hours
5	R_2	Me	18%	24%	7 days

ND = not detected

Scheme 2. Room temperature H/D exchange for selected ligands (for more details see ESI Table S2).

For **L1-NMe$_2$** H/D exchange did occur, albeit very slowly, at room temperature. However, with **L1-OMe** no deuterium incorporation was detected after 10 days at room temperature. Similar experiments were carried out with some *meta*-substituted ligands **L2-R**. H/D exchange with **L2-NMe$_2$** was much faster than with **L1-NMe$_2$** with >50% exchange within 2 hours. Surprisingly exchange occurs in both sites even though no formation of the *ortho* isomer was observed in the preparative reaction. For **L2-OMe** and **L2-Me** H/D exchange is slower than with **L2-NMe$_2$** but again occurs in both positions even though **2-Me** is not observed as a product in the preparative reaction. The H/D exchange reactions show that *ortho*-C–H activation is accessible even in cases where no *ortho* cyclometallated product is formed.

To investigate the relative rates of cyclometallation with the differently substituted ligands competition reactions were carried out (Scheme 3) and the results of individual experiments are shown in the ESI Tables S3 and S4.

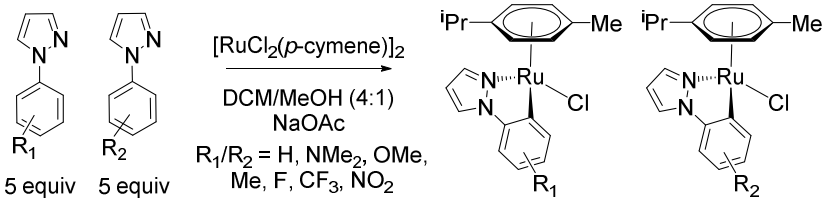

Scheme 3. Competition experiments to establish selectivity (for results of individual experiments see ESI Tables S3 and S4)

The initial ratios at room temperature were measured after 15 minutes (reactions with very electron withdrawing groups required longer to reach measurable conversion) and these values were taken as indicative of kinetic selectivity. The relative rates of reaction with the various substituents are shown in Tables S3 and S4 and the Hammett plot is shown in Figure 2. As can be seen, a good straight line

(correlation = 0.96) with a negative slope (-2.4) was obtained when using σ_m and σ_p. The negative slope arises from faster reactions with electron donating substituents and is characteristic of a cationic intermediate with some build-up of positive charge in the transition state. A plot using σ_m^+ and σ_p^+ (see **Fig. S2**) showed a significantly worse straight line with a correlation of 0.87 providing evidence against an S_EAr mechanism. The slope of -2.4 is very similar to those found in related reactions with $[MCl_2Cp^*]_2$ (M = Ir, Rh) (-2.7 and -2.3 for Ir and Rh respectively) which were ascribed to an AMLA/CMD mechanism.[22]

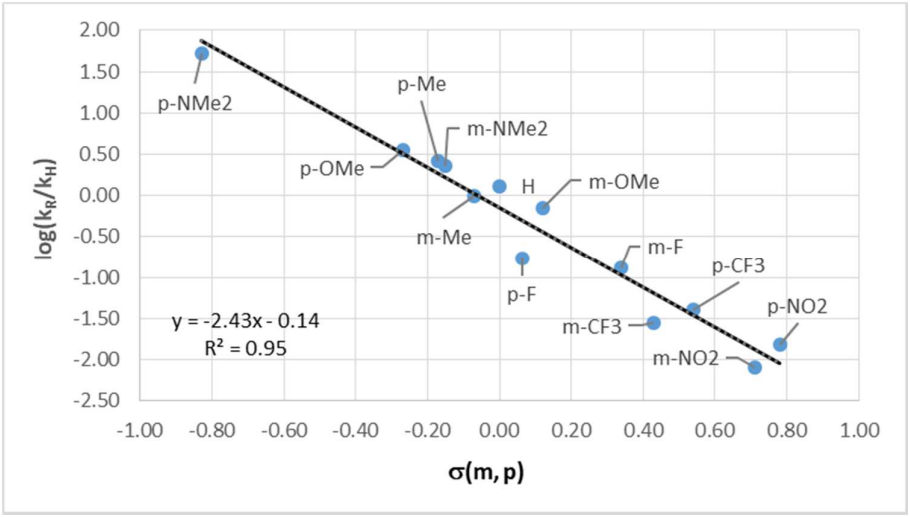

Figure 2 Hammett plot of log (k_R/k_H) for formation of *meta* and *para*-substituted complexes of Ru against σm and σp.

As mentioned above some of the *ortho*:*para* ratios changed over time and the deuteration experiments suggested that at least some reactions are reversible at room temperature. To probe the thermodynamic selectivity the competition experiments were heated, if necessary with pivalic acid, to promote reversibility.[26] The results are plotted as log(K_R/K_H) (K_R/K_H = equilibrium ratio with respect to H) versus the Hammett parameter (Figure 3) and show a reasonable straight line[27] but now with a positive slope demonstrated that ligands with more positive Hammett values (i.e. with electron withdrawing substituents) are the more thermodynamically stable products. This is entirely opposite to the kinetic selectivity for which electron donating groups are favored. This reversal of selectivity shows that a single mechanism can favour either electron donating groups or electron withdrawing groups based on the reaction conditions.

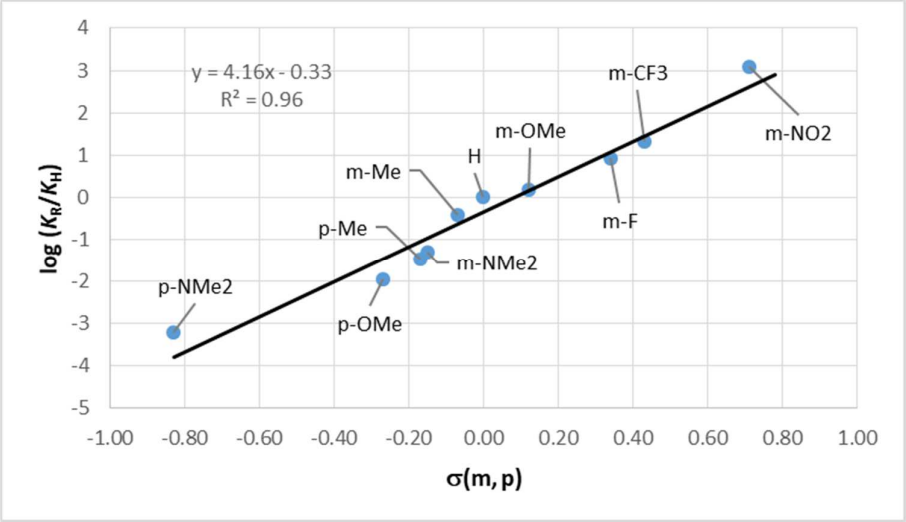

Figure 3: Hammett plot of log(K_R/K_H) for formation of *meta* and *para*-substituted complexes of Ru against σ_m and σ_p.

Computational Studies

Kinetic and Thermodynamic Selectivities. DFT calculations were employed to define the mechanisms associated with these cyclometallation reactions. The calculations were based on our previously published protocol[21] with optimised geometries and thermodynamic corrections computed with the BP86 functional, with further corrections for basis set, dispersion and solvation effects. The choice of solvent in the calculations had a significant effect on the computed energetics. Experimentally the competition reactions were carried out in 4:1 mixtures of DCM:methanol. Continuum solvation corrections were therefore assessed for both pure methanol (ε = 32.6) and pure DCM (ε = 8.93). The computed results in methanol tend to give lower barriers that were more compatible with the reversibility seen in some of the cyclometallation processes. In addition, in previous work with [$RuCl_2$(*p*-cymene)]$_2$ we have found that that even a few equivalents of MeOH in DCM is enough to promote loss of chloride, possibly due to specific solvation effects.[28] We therefore present the results computed in methanol and provide the equivalent data computed in dichloromethane in the ESI. Importantly, the trends in reactivity discussed below are independent of solvent choice.

The initial reaction of the [$RuCl_2$(*p*-cymene)]$_2$ dimer (**A**) with NaOAc can form either [RuCl(OAc)(*p*-cymene)] (**B**) or [$Ru(OAc)_2$(*p*-cymene)] (**C**) and, as noted above, we found chloride species **B** to persist during the preparative cyclometallation reactions. In the absence of added ligand, reaction of [RuCl(OAc)(*p*-cymene)] with excess NaOAc in MeOH slowly forms [$Ru(OAc)_2$(*p*-cymene)], **C**, over time, suggesting the latter is thermodynamically more stable.[29] However, given this slow rate of Cl/OAc exchange we have assumed [RuCl(OAc)(*p*-cymene)] to be the dominant species present prior

to reaction was the added ligands. Therefore in the following all free energies are quoted relative to the combined energies of **B** with any necessary ligands set to 0.0 kcal/mol.[30]

Computed free energy profiles for the reactions of ligands **L2-NMe$_2$** and **L2-NO$_2$** with **B** to generate the *para*-substituted products **3-NMe$_2$** and **3-NO$_2$** are shown in Figure 4. Addition of **L2-NMe$_2$** to **B** can give either $\mathbf{D}_o$ (at -3.0 kcal/mol, as shown) or $\mathbf{D}_p$ (at -1.9 kcal/mol) in which the *para*-NMe$_2$ substituent is rotated away from the metal centre. As interconversion between these two species is likely to be accessible[31] we have taken $\mathbf{D}_o$ to be the most stable precursor and this species is used in the calculation of the energy span.[32] Rearrangement to $\mathbf{D}_p$ and acetate dissociation generates $\mathbf{E}_p$ at -0.8 kcal/mol from which C–H activation proceeds in two steps, the first being the κ^2-κ^1 displacement of acetate to form an agostic intermediate, **Int(E-F)**$_p$, at +7.0 kcal/mol. The C–H bond in **Int(E-F)**$_p$ is thus polarized, allowing for its facile deprotonation by the pendant arm of the κ^1-OAc ligand to give an initial cyclometallated species, $\mathbf{F}_p$, at +2.5 kcal/mol. Dissociative substitution of HOAc by Cl^- proceeds via 16e $\mathbf{F1}_p$ at +9.9 kcal/mol to give $\mathbf{G}_p$ (equivalent to **3-NMe$_2$** in the experimental study) at -5.4 kcal/mol. The reaction therefore proceeds with an overall barrier of 14.7 kcal/mol in which **TS(E-F)1**$_p$ is rate-limiting. The reverse reaction entails a barrier of 17.1 kcal/mol.[33] Note that we have not attempted to compute transition states for the dissociation of HOAc from $\mathbf{F}_p$, or for Cl^- addition to $\mathbf{F1}_p$ to form $\mathbf{G}_p$ and we return to this point in the Discussion section.

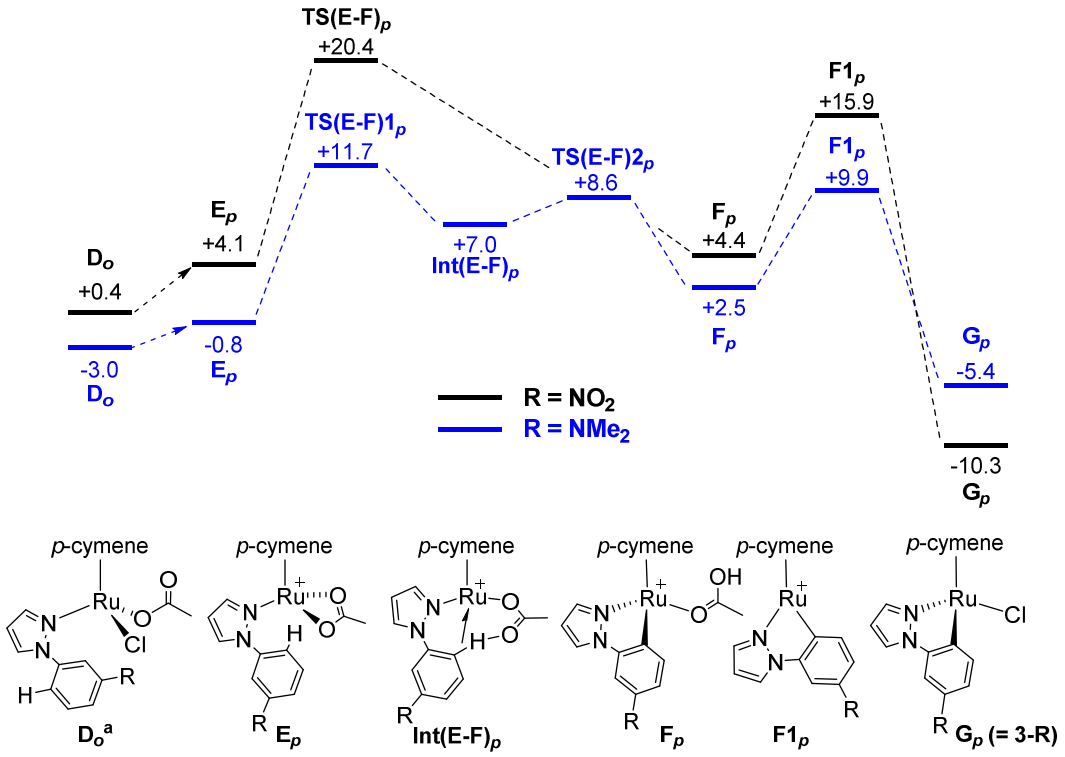

Figure 4. Computed free energy profiles (kcal/mol) for the reactions of **L2-NMe$_2$** (blue) and **L2-NO$_2$** (black) at [RuCl$_2$(*p*-cymene)]$_2$. Free energies are quoted relative to [Ru(Cl)(OAc) (*p*-cymene)] (**B**) and

the free ligand set to 0.0 kcal/mol. [a]The more stable $\mathbf{D}_o$ rotamers are shown; $\mathbf{D}_p$ is located at -1.9 kcal/mol for **L2-NMe$_2$** and at +0.6 kcal/mol for **L2-NO$_2$**.

With **2-NO$_2$** a similar reaction profile is computed with the exception that no agostic intermediate is located. C–H activation therefore proceeds in one step from $\mathbf{E}_p$ via **TS(E-F)$_p$** at +20.4 kcal/mol. This represents a significantly higher overall barrier and reflects several accumulative effects: (i) less favourable ligand binding to form $\mathbf{D}_o/\mathbf{D}_p$; (ii) harder acetate loss to form $\mathbf{E}_p$, and (iii) a more difficult C–H activation step. Conversely, HOAc/Cl$^-$ substitution is much more favourable and gives $\mathbf{G}_p$ (i.e. **3-NO$_2$**) at -10.3 kcal/mol. Formation of **3-NO$_2$** is therefore computed to be favoured thermodynamically over **3-NMe$_2$**, but the latter is favoured kinetically. This nicely captures the experimental observations that indicate the particular outcome will depend on the reaction conditions.

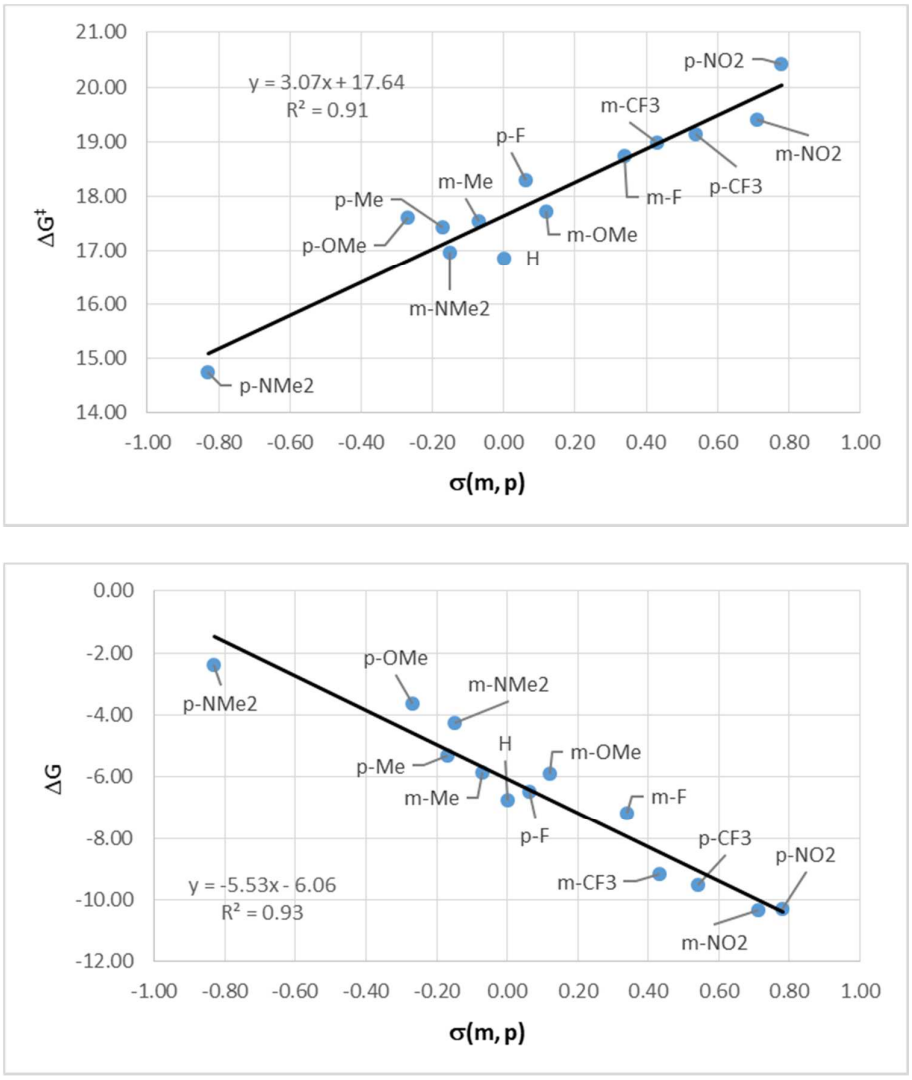

Figure 5. Plots of computed values of $\Delta G^{‡}$ and ΔG (kcal/mol) against σ_m and σ_p Hammett constants for the reactions of **L1-R** and **L2-R** to form **1-R** and **3-R**.

Extending the above study to the remaining **L2-R** ligands and the set of *para*-substituted **L1-R** ligands (that give *meta*-substituted products **1-R**) allowed us to define overall free energy barriers, $\Delta G^{\ddagger}$, and overall free energy changes for product formation, ΔG, in each case. Plots of $\Delta G^{\ddagger}$ and ΔG against the appropriate Hammett parameters are shown in Figure 5 and in both cases reasonable correlations with $R^2 > 0.91$ are found. Most importantly these extended data sets reiterate the opposing trends seen experimentally, with products featuring electron-withdrawing substituents being favoured thermodynamically, while those with more electron-donating substituents are kinetically favoured. Overall this means that substrates featuring the most electron-donating substituents will be most likely to exhibit reversible C–H activation. Experimentally H/D exchange is seen with **L2-NMe$_2$**, **L2-OMe**, **L2-Me** and **L1-NMe$_2$** and computationally these do exhibit the lowest activation barriers for the reverse proto-demetallation (17.1 kcal/mol, 21.3 kcal/mol, 22.8 kcal/mol and 21.2 kcal/mol, respectively).

An external deprotonation mechanism was also assessed for all ligands, and transition states for this process in methanol were found to lie between 3 and 7 kcal/mol above those for intramolecular C–H activation. In dichloromethane, in contrast, external deprotonation becomes competitive, in particular for ligands bearing electron-withdrawing groups. However, whereas plots of $\Delta G^{\ddagger}$ and ΔG against Hammett parameter provided excellent correlations when based on the intramolecular transition states computed in dichloromethane ($R^2 = 0.91$ and 0.95 respectively), a similar plot based on the external deprotonation gives a poor correlation ($R^2 = 0.63$, see ESI). This may be taken as evidence that external deprotonation is not occurring in these systems. However, we suggest that the presence of 20% methanol in the mixed DCM/methanol solvent system used experimentally is sufficient to reduce the barriers to intramolecular C–H activation such that the computed results in methanol provide a more appropriate fit to the experimental results. Indeed, computed barriers for intramolecular C–H activation are 6-9 kcal/mol lower in methanol and most of this difference can be ascribed to the easier dissociation of Cl^- to form precursor $\mathbf{E}_{\boldsymbol{p}}$.

***Ortho* C–H Activation.** Pathways for *ortho*-C–H activation in **L2-NMe$_2$**, **L2-OMe**, **L2-Me** and **L2-F** were computed to account for the *ortho*-H/D exchange and the time-dependent *ortho:para* ratios observed with **L2-OMe** and **L2-F**. Truncated computed profiles highlighting the key stationary points governing the overall energetics of these processes are presented in Figure 6, along with the equivalent plots for the competing *para*-C–H activations. In all cases the thermodynamic preference seen experimentally is reproduced by the calculations, with *ortho*-substituted products favoured with **L2-OMe** and **L2-F** and the *para*-substituted products with **L2-NMe$_2$** and **L2-Me**. An important additional factor in accounting for the selectivities is the high energy of $\mathbf{F1}_{\boldsymbol{o}}$ computed with **L2-NMe$_2$** and **L2-Me**. This reflects a steric clash between these larger *ortho* substituents and the *p*-cymene ring.

As a result the HOAc dissociation step becomes kinetically relevant and has the effect of increasing the overall barrier to *ortho*-C–H activation. The formation of the *para*-substituted products, **3-Me** and **3-NMe$_2$**, is therefore favoured kinetically as well as thermodynamically, as seen experimentally. With the sterically less demanding **L2-F** and **L2-OMe** ligands C–H activation is rate-limiting for both the *ortho*- and *para*-pathways: for **L2-OMe TS(E-F)$_o$** is favoured by 0.7 kcal/mol, consistent with the small experimental preference for the formation of **2-OMe** over **3-OMe** at short timescales. With **L2-F TS(E-F)$_p$** is 0.2 kcal/mol more stable than **TS(E-F)$_o$**, and appears to be inconsistent with the preferential formation of **2-F** at short reaction times. However, the *ortho*- and *para*-C–H activation pathways are clearly kinetically competitive. The situation may also be further complicated by the energetic proximity of intermediates **F1** to the C–H activation transition states **TS(E-F)** and we return to this point in the Discussion section below.

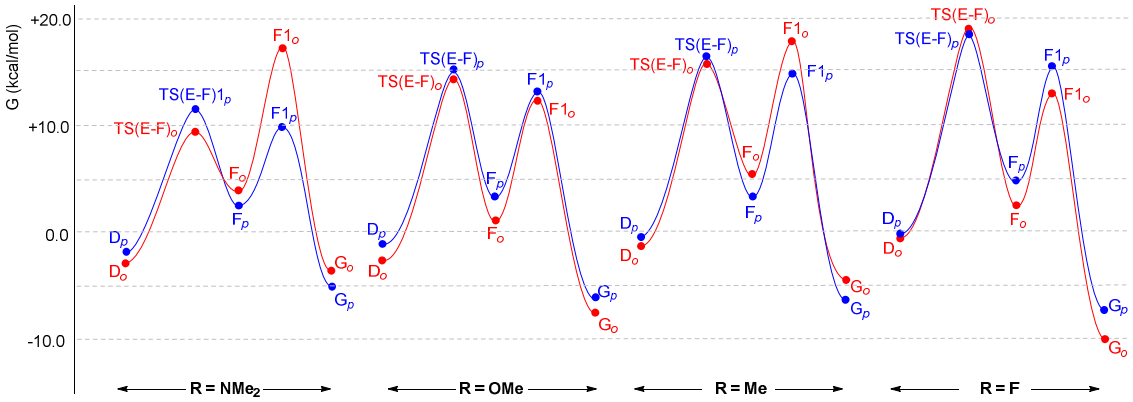

Figure 6. Computed free energy profiles (kcal/mol) for the cyclometallation reactions of **L2-R** at [Ru(OAc)Cl(*p*-cymene)]; *ortho*-C–H activation shown in red and *para*-C–H activation in blue.

The reaction profiles in Figure 6 indicate that *ortho*-H/D exchange in the ligand could occur either via (i) *ortho*-C–H bond cleavage via **TS(E-F)$_o$** to form **F$_o$**, followed by H/D exchange with solvent at **F$_o$** to form a bound AcOD ligand and subsequent deutero-demetallation, or (ii) formation of **G$_o$** (i.e. **2-R**) and free AcOH, H/D exchange with solvent to form AcOD, which then reverses the overall cyclometallation process. This analysis makes an important distinction between the C–H bond activation event (to form **F$_o$**) and the overall cyclometallation process (to form **G$_o$**/**2-R**). Indeed *ortho*-C–H bond cleavage is surprisingly accessible even in the presence of bulky *ortho*-NMe$_2$ and -Me substituents. The fact that no *ortho*-cyclometallated products are seen with these ligands is more in line with the general expectation that *ortho:para* selectivities are dominated by steric effects. In our computed profiles this steric selectivity only becomes apparent after the C–H bond cleavage event, presumably as any steric impact only becomes sufficient to play a role once the Ru–aryl bond is in

place. Indeed the very same steric effect may be responsible for facilitating the κ^2-κ^1-dissociation of the acetate ligand that is a major component of the C–H activation process via **TS(E-F)$_o$** and thus making *ortho*-C–H bond cleavage more accessible (see the transition state analysis below). For **L2-F** and **L2-OMe** electronic factors are more prevalent and an *ortho*-F effect has been invoked to account for the thermodynamic preference for C–H activation *ortho* to F[34] and also appears to be relevant for other electronegative substituents such as OMe.

Analysis of Rate-Limiting Transition States. The rate-limiting transition states for the C–H activation of **L2-NMe$_2$** and **L2-NO$_2$** were considered in more detail using a combination of Quantum Theory of Atoms in Molecules (QTAIM),[35] Non-Covalent Interaction (NCI) plots[36] and Natural Bond Orbital (NBO) analyses.[37] The results are shown in Figure 7, which also includes the parent **L-H** ligand for comparison. **L-H** undergoes a one-step C–H activation similar to that characterised for **L2-NO$_2$**.

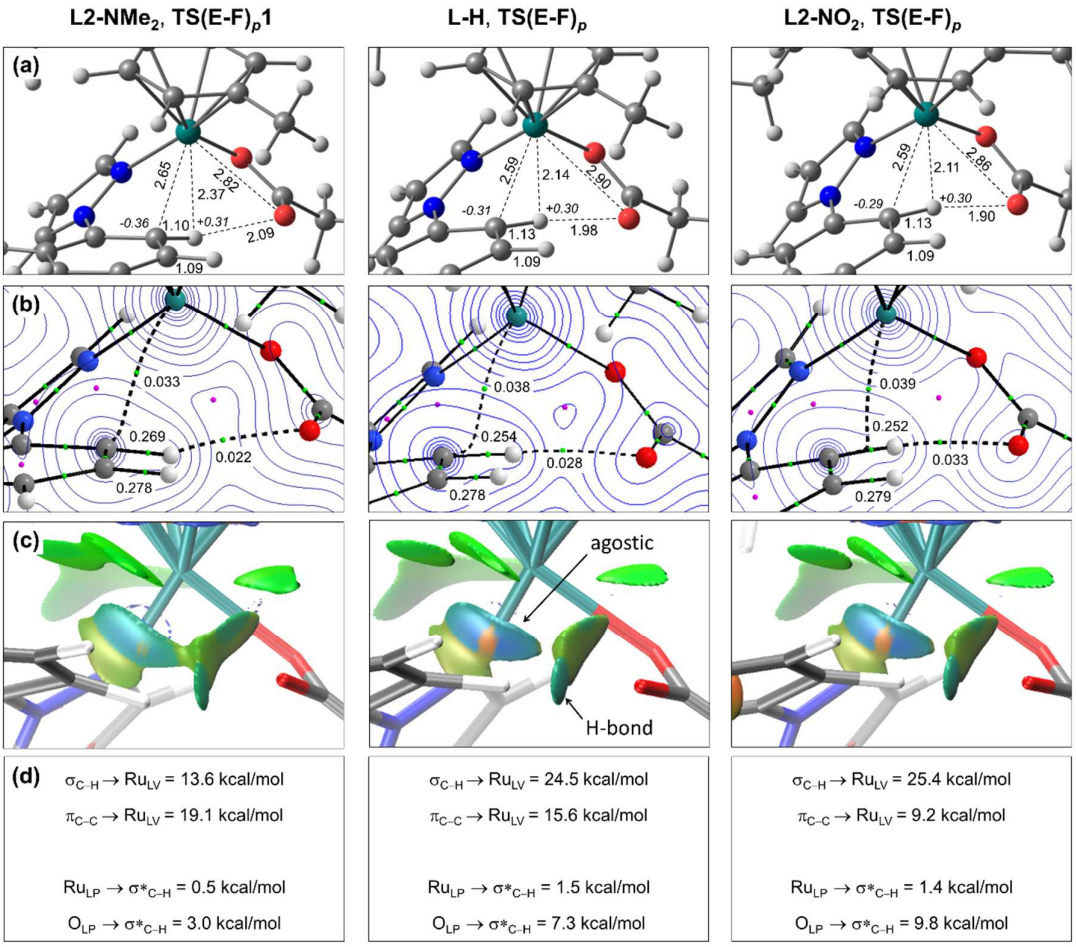

Figure 7. Analysis of rate-limiting transition states for the C–H activation of **L2-NMe$_2$**, **L-H** and **L2-NO$_2$**. (a) Computed geometries with selected distances in Å (plain text) and computed NBO atomic charges at the activating C–H bond (in italics); (b) QTAIM molecular graphs: contours are plotted in

the Ru–C^{ortho}–H^{ortho} plane; BCPs and RCPs are shown as green and pink spheres respectively, with selected BCP electron densities, ρ(r), in eÅ^{-3}; (c) NCI plots: isosurfaces generated for s = 0.3 au and $-0.07 < \rho < 0.07$ au; (d) Key donor-acceptor interactions from NBO 2nd order perturbation analyses.

For all three ligands the major feature of the rate-limiting transition state is associated with the κ^2-κ^1-displacement of the OAc ligand, with the Ru–O bond elongating from ca. 2.15 Å in the precursor intermediates **E**$_p$ to over 2.8 Å in the transition states. As this occurs the phenyl ring of the ligand approaches the metal centre, although the Ru···C^{ortho} contacts are still long at ca. 2.6 Å. All three transition states are 'early' in that they have minimal C–H bond elongation (1.10 – 1.13 A), with a trend towards shorter Ru···H^{ortho} and H^{ortho}···O distances discernible from **L2-NMe$_2$** through **L2-H** to **L2-NO$_2$**. Despite this some polarization of the *ortho*-C–H bonds is seen, in particular through increased negative charge on C^{ortho}.[38] These general features are reflected in the QTAIM molecular graphs in Figure 7(b). These show Ru···C^{ortho} and H^{ortho}···O bond paths, but these represent weak interactions at this point, as evidenced by low bond critical point (BCP) electron densities, ρ(r). The C^{ortho}–H^{ortho} bonds are only slightly perturbed in these transition states, with ρ(r) values marginally lower than the adjacent spectator C^{meta}–H^{meta} bonds. The bond paths around the Ru···C^{ortho}–H^{ortho}-···O–C–O moiety encircle a ring critical point (RCP) and graphically illustrate the 6-membered nature of these AMLA-6 transition states.[39] The Ru···C^{ortho} bond paths also show increased curvatures near C^{ortho} along the series; this feature usually reflects electron deficiency and so correlates with the trend from the electron-donating *p*-NMe$_2$ substituent to the electron withdrawing *p*-NO$_2$ group.

More insight into these interactions can be seen in the NCI plots in Figure 7(c). NCI plots highlight regions of weak interactions and are colour coded, with stronger stabilising interactions in blue, weaker stabilising interactions in green and stronger destabilising areas in red. The main features are highlighted in Figure 7(c) for **L-H**. Firstly, the presence of a light blue disk along the H^{ortho}···O bond path indicates the presence of hydrogen bonding. Secondly, the Ru···C^{ortho}–H^{ortho} interaction is shown in the much broader (stabilising) turquoise feature, which is interrupted by a red region that aligns with the centre of the C^{ortho}–H^{ortho} bond. This indicates an area of destabilising charge depletion and this stabilising-destabilising-stabilising pattern highlights that both the C^{ortho} and H^{ortho} centres are interacting with the Ru to give an $\eta^2_{C–H}$→Ru agostic bond. Similar patterns have been noted in Rh σ-alkane complexes[40] and Rh and Ag σ-amineborane[41] complexes. Thus these NCI plots can enhance the bonding information emerging from the more localised BCP and RCP data of the QTAIM study.[42]

The NCI plot for **L2-NO$_2$** is very similar to that for **L-H**, but for **L2-NMe$_2$** both the agostic and H-bonding features are less well defined. The reasons for this can be seen in the donor-acceptor interactions provided by the NBO 2nd order perturbation analysis (see Figure 7(d)). For the parent **L-H** system the largest interaction (24.5 kcal/mol) involves $\sigma_{C–H}$→Ru σ-donation. Ru→$\sigma^*_{C–H}$ back-bonding is fairly limited, however, significant donation from the O lone pairs into the $\sigma^*_{C–H}$ orbital is

computed (7.3 kcal/mol). An additional significant interaction is also seen in donation from a $\pi_{C=C}$ orbital on the phenyl ring to Ru (15.6 kcal/mol). This contribution has been termed 'syndetic bonding' by Nielson and Schwerdtfeger in their studies on agostic bonding[43] and the cyclometallation of dimethylbenzylamine at $Pd(OAc)_2$.[44] The weightings of the agostic, H-bonding and syndetic contributions vary with the *para* substituent: for **L2-NMe$_2$** the syndetic term is enhanced (19.1 kcal/mol) while $\sigma_{C-H} \rightarrow$Ru donation and $O_{LP} \rightarrow \sigma^*_{C-H}$ donation are diminished (13.6 kcal/mol and 3.0 kcal/mol respectively); with **L2-NO$_2$** the opposite is seen, with $\sigma_{C-H} \rightarrow$Ru and $O_{LP} \rightarrow \sigma^*_{C-H}$ donation increasing to 25.4 kcal/mol and 9.8 kcal/mol respectively, while the syndetic term falls to 8.2 kcal/mol.

Discussion.

The key outcome of this study is to highlight how the use of ligand substituent effects to interpret the detailed mechanism of a C–H activation process may depend crucially on the reaction conditions employed. This reinforces the outcomes of our previous study on related $[MCl_2Cp^*]_2$ systems (M = Rh, Ir).[22] For the current 1-phenylpyrazole systems stoichiometric cyclometallation at Ru is enhanced by electron-donating substituents when under kinetic control, or favoured by electron-withdrawing substituents when under thermodynamic control. When considering catalytic systems, the role of the C–H activation within the overall cycle must also be considered: is the C–H activation overall rate-limiting, or is it a pre-equilibrium step prior to a later rate-limiting functionalisation process? If the former, a substituent effect would reflect kinetic control, but for the latter the C–H activation would be reversible and so any substituent effect might reflect thermodynamic control. In the latter scenario the effects of substituents on the steps later in the catalytic cycle also need to be considered.

Defining the role of C–H activation within a catalytic cycle is usually addressed via H/D exchange and k_H/k_D KIE experiments. For the former it is important to consider H/D exchange both in the presence and the absence of coupling partner substrates, while a significant k_H/k_D KIE will indicate that C–H activation is rate-limiting. However, if a k_H/k_D KIE is not observed it does not necessarily mean that C–H activation is not rate-limiting. This is evident in the rate-limiting transition states computed in this study; these exhibit very early transition state geometries with minimal C–H bond elongation and hence would not be expected to show a significant k_H/k_D KIE. We have previously demonstrated this both computationally and experimentally for the Ru-catalysed coupling of 3-phenylpyrazole with alkynes.[6g]

The transition state analyses draw on a number of electronic structure techniques to highlight the agostic and H-bonding interactions that are central to the AMLA concept. In particular "AMLA" emphasizes how these two components work together synergically to cleave C–H bonds.[7a] This picture is added to by the syndetic bonding term, and our present study highlights how these three components vary depending on the nature of ligand substrate. Thus the single AMLA/CMD

mechanism can accommodate a range of ligand substrates of differing electronic character. The present substituted 1-phenylpyrazole ligands all react via an AMLA/CMD process that is favoured by electron-releasing substituents when under conditions of kinetic control, or by electron-withdrawing substituents when under thermodynamic control. While this pattern is observed for the current system, other metal/substrate combinations have been shown to proceed by an AMLA/CMD pathway that are favoured both kinetically and thermodynamically with electron-withdrawing groups.[9, 20a, 45]

The characterisation of C–H activation processes as following a BIES mechanism is usually founded on the observation that electron-donating substituents enhance reactivity, but our present and previous studies[21,22] suggest this can also be consistent with an AMLA/CMD process. Indeed in our view BIES is indistinguishable from AMLA/CMD. Moreover, the use of the descriptor 'electrophilic' is potentially unhelpful as it could be associated with an S_EAr process, and thus not to apply to reactions which are favoured by electron-withdrawing substituents. Factors other than C–H bond cleavage may also contribute to the overall C–H activation barrier. In the present cyclometallation reactions, the interactions involving the C–H bond in the rate-limiting transition states are all relatively weak and the major geometric change required to access the C–H bond cleavage transition state involves Ru–O bond dissociation. In addition, both this process and the initial ligand binding and anion dissociation steps (**B** → **D** and **D** → **E**) all contribute to the energy span that corresponds to the overall activation barriers, $\Delta G^{\ddagger}$. Given that all three of these factors are promoted by electron-releasing substituents this likely accounts for the good correlations seen in the kinetic Hammett plots both experimentally and computationally.

Another feature of the computed pathways is the potential kinetic relevance of the formation and onward reaction of 16e intermediates such as **F1** (see Figure 6). In general, the details of any ligand loss and substitution processes have been overlooked in previous studies[7b] and this may be due, at least in part, to the difficulties in computing barriers for such processes. We have also not attempted to compute this here, however, assuming addition of HOAc or Cl^- to **F1** (to form **F** or **G** respectively) is diffusion-controlled with a rate $k = 1 \times 10^{10}$ $M^{-1}s^{-1}$ equates at room temperature to an additional barrier of 3.8 kcal/mol above **F1**. Thus intermediates such as **F1** do not even represent a lower limit to the substitution barrier. Moreover, the free energy of **F1** will have a strong entropic component that is known to be difficult to quantify with static gas-phase calculations.[46] This discussion also assumes that a purely dissociative ligand substitution mechanism is valid.[47] Ultimately the modelling of such processes will need to capture important specific solvation effects that require the development of efficient protocols to allow the use of more realistic chemical models and thus to provide improved physical insights into mechanistic processes in organometallic chemistry.

Conclusions.

We have presented a joint experimental and computational mechanistic study on the cyclometallation reactions of substituted 1-phenylpyrazoles at $[RuCl_2(p\text{-cymene})]_2$. The results show that a single C–H activation process may show contradictory substituent effects depending on the reaction conditions: under kinetic control ligands with electron-releasing substituent are favoured, whereas the opposite trend is seen under thermodynamic control. The reaction conditions must therefore be taken into account when using substituent effects to infer details about the mechanism of C–H activation. Moreover in catalysis the role of the C–H activation process within the catalytic cycle must also be considered. A detailed analysis of the rate-limiting transition states reveals an AMLA/CMD process with synergic contributions from agostic and H-bonding interactions. These are complemented by a syndetic bonding term, and the contributions of these three components are found to vary in a complementary fashion depending on the nature of the substituent. The major geometric change required to access the transition states involves the κ^2-κ^1 displacement of the acetate ligand with significant Ru–O bond elongation. These transition states therefore exhibit minimal C–H bond elongation and so would not be expected to show a significant k_H/k_D KIE. The overall energy span also involves ligand addition and Cl^- dissociation, all of which are promoted by electron-releasing substituents. H/D exchange studies and computed reaction profiles reveal a surprising kinetic accessibility for *ortho*-C–H bond activation, even in cases where no *ortho*-cyclometalated product is observed. The kinetic relevance of HOAc/Cl^- ligand substitution via a 16e intermediate is identified and the accurate modelling such processes is identified as a future challenge for computational chemistry.

Acknowledgements.

We thank the EPSRC for financial support through awards EP/ J002712/1 and EP/J021911/1 (S.A.M.) and EP/J002917/1 and EP/J021709/1 (D.L.D.) and EUCOST Action CA15106 "C−H Activation in Organic Synthesis (CHAOS)". RAA thanks the Iraq government for a scholarship.

Electronic Supplementary Information (ESI) available: Crystallographic data (CIF), full experimental details, NMR spectra, and details of all computed reaction profiles, energies, NBO analyses and Cartesian coordinates. CCDC 1913188-1913192 contain complete crystallographic data for this paper and these data can be obtained free of charge from the Cambridge Crystallographic Data Centre via http://www.ccdc.cam.ac.uk/pages/Home.aspx. See DOI: 10.1039/x0xx00000x

References.

1. L. Ackermann, *Chem. Rev.*, 2011, 111, 1315-1345.
2. P. B. Arockiam, C. Bruneau and P. H. Dixneuf, *Chem. Rev.*, 2012, 112, 5879-5918.
3. D. Zell, S. Warratz, D. Gelman, S. J. Garden and L. Ackermann, *Chem. -Eur. J.*, 2016, 22, 1248-1252.
4. (a) S. Ruiz, P. Villuendas, M. A. Ortuño, A. Lledós and E. P. Urriolabeitia, *Chem. -Eur. J.*, 2015, 21, 8626–8636; (b) C. Tirler and L. Ackermann, *Tetrahedron*, 2015, 71, 4543-4551; (c) A. S.

Trita, A. Biafora, M. Pichette Drapeau, P. Weber and L. J. Gooßen, *Angew. Chem., Int. Ed.*, 2018, 57, 14580-14584; (d) Y. Xie, X. Wu, C. Li, J. Wang, J. Li and H. Liu, *J. Org. Chem.*, 2017, 82, 5263-5273.

5. (a) M. Simonetti, R. Kuniyil, S. A. Macgregor and I. Larrosa, *J. Am. Chem. Soc.*, 2018, 140, 11836-11847; (b) M. Simonetti, G. J. P. Perry, X. C. Cambeiro, F. Juliá-Hernández, J. N. Arokianathar and I. Larrosa, *J. Am. Chem. Soc.*, 2016, 138, 3596-3606.
6. (a) N. Y. P. Kumar, T. Rogge, S. R. Yetra, A. Bechtoldt, E. Clot and L. Ackermann, *Chem. -Eur. J.*, 2017, 23, 17449-17453; (b) J. McIntyre, I. Mayoral-Soler, P. Salvador, A. Poater and D. J. Nelson, *Cat. Sci. Tech.*, 2018, 8, 3174-3182; (c) J. A. Leitch, P. B. Wilson, C. L. McMullin, M. F. Mahon, Y. Bhonoah, I. H. Williams and C. G. Frost, *ACS Catal*, 2016, 6, 5520-5529; (d) S. Jambu, M. Tamizmani and M. Jeganmohan, *Org. Lett.*, 2018, 20, 1982-1986; (e) A. Anukumar, M. Tamizmani and M. Jeganmohan, *J. Org. Chem.*, 2018, 83, 8567-8580; (f) S. Dana, D. Chowdhury, A. Mandal, F. A. S. Chipem and M. Baidya, *ACS Catal*, 2018, 8, 10173-10179; (g) A. G. Algarra, W. B. Cross, D. L. Davies, Q. Khamker, S. A. Macgregor, C. L. McMullin and K. Singh, *J. Org. Chem.*, 2014, 79, 1954-1970.
7. (a) Y. Boutadla, D. L. Davies, S. A. Macgregor and A. I. Poblador-Bahamonde, *Dalton Trans.*, 2009, 5820-5831; (b) D. L. Davies, S. A. Macgregor and C. L. McMullin, *Chem. Rev.*, 2017, 117, 8649−8709.
8. (a) A. Gray, A. Tsybizova and J. Roithova, *Chem. Sci.*, 2015, 6, 5544-5553; (b) Y.-H. Sun, T.-Y. Sun, Y.-D. Wu, X. Zhang and Y. Rao, *Chem. Sci.*, 2016, 7, 2229-2238.
9. D. Lapointe and K. Fagnou, *Chem. Lett.*, 2010, 39, 1119-1126.
10. D. H. Ess, S. M. Bischof, J. Oxgaard, R. A. Periana and W. A. Goddard, *Organometallics*, 2008, 27, 6440-6445.
11. E. F. Flegeau, C. Bruneau, P. H. Dixneuf and A. Jutand, *J. Am. Chem. Soc.*, 2011, 133, 10161-10170.
12. I. Fabre, N. von Wolff, G. Le Duc, E. F. Flegeau, C. Bruneau, P. H. Dixneuf and A. Jutand, *Chem. -Eur. J.*, 2013, 19, 7595-7604.
13. L. Zhang, L. Yu, J. Zhou and Y. Chen, *Eur. J. Org. Chem.*, 2018, 2018, 5268-5277.
14. D. L. Davies, S. M. A. Donald and S. A. Macgregor, *J. Am. Chem. Soc.*, 2005, 127, 13754-13755.
15. (a) W. Ma, R. Mei, G. Tenti and L. Ackermann, *Chem. -Eur. J.*, 2014, 20, 15248-15251; (b) R. Mei, S.-K. Zhang and L. Ackermann, *Org. Lett.*, 2017, 19, 3171-3174; (c) K. Raghuvanshi, K. Rauch and L. Ackermann, *Chem. -Eur. J.*, 2015, 21, 1790-1794; (d) K. Raghuvanshi, D. Zell, K. Rauch and L. Ackermann, *ACS Catal*, 2016, 6, 3172-3175; (e) L. Su, Z. Yu, P. Ren, Z. Luo, W. Hou and H. Xu, *Org. Biomol. Chem.*, 2018, 16, 7236-7244; (f) Q. Bu, T. Rogge, V. Kotek and L. Ackermann, *Angew. Chem., Int. Ed.*, 2018, 57, 765-768.
16. L. Ackermann, A. V. Lygin and N. Hofmann, *Angew. Chem., Int. Ed.*, 2011, 50, 6379-6382.
17. X. Wu, B. Wang, S. Zhou, Y. Zhou and H. Liu, *ACS Catal*, 2017, 7, 2494-2499.
18. R. K. Rit, K. Ghosh, R. Mandal and A. K. Sahoo, *J. Org. Chem.*, 2016, 81, 8552-8560.
19. S. I. Gorelsky, D. Lapointe and K. Fagnou, *J. Am. Chem. Soc.*, 2008, 130, 10848-10849.
20. (a) S. I. Gorelsky, D. Lapointe and K. Fagnou, *J. Org. Chem.*, 2012, 77, 658-668; (b) S. I. Gorelsky, *Coord. Chem. Rev.*, 2013, 257, 153-164.
21. K. J. T. Carr, S. A. Macgregor, D. L. Davies, K. Singh and B. Villa-Marcos, *Chem. Sci.*, 2014, 5, 2340-2346.
22. R. A. Alharis, C. L. McMullin, D. L. Davies, K. Singh and S. A. Macgregor, *J. Am. Chem. Soc.*, 2019, http://dx.doi.org/10.1021/jacs.9b02073.
23. Y. Boutadla, D. L. Davies, R. C. Jones and K. Singh, *Chem. -Eur. J.*, 2011, 17, 3438-3448.
24. D. A. Tocher, R. O. Gould, T. A. Stephenson, M. A. Bennett, J. P. Ennett, T. W. Matheson, L. Sawyer and V. K. Shah, *J. Chem. Soc., Dalton Trans.*, 1983, 1571-1581.
25. J. Milani, N. E. Pridmore, A. C. Whitwood, I. J. S. Fairlamb and R. N. Perutz, *Organometallics*, 2015, 34, 4376-4386.

26. (a) Systems featuring the Ru(*p*-cymene)$^{2+}$ fragment can also show a propensity for arene dissociation, especially in stronger donor solvents.[5b, 6b, 11, 26b] The arene stays bound here even in some cases upon prolonged heating. Note that the conclusions drawn here may not necessarily transfer to systems where arene dissociation does occur; (b) S. Fernandez, M. Pfeffer, V. Ritleng and C. Sirlin, *Organometallics*, 1999, 18, 2390-2394.
27. Obtaining data for the full **L2-R** ligand series was problematic due to the *ortho*-F product, **2-F**, being considerably favoured over the *para*-F product, **3-F**. These data were therefore unreliable, as are those for the formation of **3-CF$_3$** and **3-NO$_2$** which rely on the data for **3-F** . In addition achieving equilibrium required heating for long periods and leads to some decomposition. With these points included the R^2 value dropped to 0.87.
28. D. L. Davies, O. Al-Duaij, J. Fawcett and K. Singh, *J. Organomet. Chem.*, 2008, 693, 965-980.
29. (a) A recent kinetic study has shown that reaction of [RuCl$_2$(*p*-cymene)]$_2$ with NaOAc in acetic acid leads to the formation of [RuCl(OAc)(p-cymene)]. See Ref 29(b); (b) R. Salvio, F. Julia-Hernandez, L. Pisciottani, R. Mendoza-Merono, S. Garcia-Granda and M. Bassetti, *Organometallics*, 2017, 36, 3830-3840.
30. Computationally we find **C** is indeed more stable than **B**, by 1.5 kcal/mol. Formation of **B** and **C** from [RuCl$_2$(*p*-cymene)]$_2$ and OAc is computed in methanol to be exergonic by 11.0 kcal/mol and 12.5 kcal/mol, respectively.
31. A transition state for rotation about the N-C^{ipso} bond was located at +9.4 kcal/mol. **D$_o$** and **D$_p$** may also to interconvert via dissociation of **L2-NMe$_2$**, rotation in the free ligand and re-association.
32. S. Kozuch and S. Shaik, *Acc. Chem. Res.*, 2011, 44, 101-110.
33. Throughout we computed the cyclometalated product, **G^{OAc}**, with OAc bound, to be slightly more stable than the chloride adduct **G** (by up to 0.8 kcal/mol). That these two species are close experimentally is evident in the mixtures formed in the absence of LiCl or if more than 1 equiv of NaOAc per Ru centre is employed.
34. E. Clot, O. Eisenstein, N. Jasim, S. A. Macgregor, J. E. McGrady and R. N. Perutz, *Acc. Chem. Res.*, 2011, 44, 333-348.
35. R. F. W. Bader, *Atoms in Molecules: A Quantum Theory*, Clarendon Press, Oxford, 1994.
36. J. Contreras-García, E. R. Johnson, S. Keinan, R. Chaudret, J.-P. Piquemal, D. N. Beratan and W. Yang, *J. Chem. Theory Comput.*, 2011, 7, 625-632.
37. E. D. Glendening, J. K. Badenhoop, A. E. Reed, J. E. Carpenter, A. J. Bohmann, C. M. Morales, C. R. Landis and F. Weinhold, Theoretical Chemistry Institute, University of Wisconsin, Madison, WI., 2013.
38. The negative charge on C^{ortho} increases by approximately 0.06 compared to **E$_p$** (data for **E$_p$**: **L2-NMe$_2$** C^{ortho} = -0.29, H^{ortho} = +0.28; **L-H**: C^{ortho} = -0.24, H^{ortho} = +0.29; **L2-NO$_2$**: C^{ortho} = -0.22, H^{ortho} = +0.29).
39. AMLA can also accommodate 4-membered transition states. For example, proton transfer onto the metal-bound oxygen of acetate or onto a monodentate ligand (alkoxide, amide) featuring a heteroatom lone pair would be characterised as AMLA-4. The latter processes have also been called 1,2-additions.[7a].
40. A. J. Martínez-Martínez, B. E. Tegner, A. I. McKay, A. J. Bukvic, N. H. Rees, G. J. Tizzard, S. J. Coles, M. R. Warren, S. A. Macgregor and A. S. Weller, *J. Am. Chem. Soc.*, 2018, 140, 14958-14970.
41. A. Johnson, A. J. Martínez-Martínez, S. A. Macgregor and A. S. Weller, *Dalton Trans.*, 2019, DOI: 10.1039/C9DT00971J.
42. J. R. Lane, J. Contreras-García, J.-P. Piquemal, B. J. Miller and H. G. Kjaergaard, *J. Chem. Theory Comput.*, 2013, 9, 3263-3266.
43. M. A. Sajjad, K. E. Christensen, N. H. Rees, P. Schwerdtfeger, J. A. Harrison and A. J. Nielson, *Dalton Trans.*, 2017, 46, 16126-16138.

44. M. A. Sajjad, J. A. Harrison, A. J. Nielson and P. Schwerdtfeger, *Organometallics*, 2018, 37, 3659-3669.
45. (a) D. García-Cuadrado, A. A. C. Braga, F. Maseras and A. M. Echavarren, *J. Am. Chem. Soc.*, 2006, 128, 1066-1067; (b) M. Lafrance, C. N. Rowley, T. K. Woo and K. Fagnou, *J. Am. Chem. Soc.*, 2006, 128, 8754-8756.
46. S. Grimme and P. R. Schreiner, *Angew. Chem., Int. Ed.*, 2018, 57, 4170-4176.
47. M. R. Meneghetti, M. Grellier, M. Pfeffer, J. Dupont and J. Fischer, *Organometallics*, 1999, 18, 5560-5570.